N88-27156

THE IMPORTANCE OF STEADY AND DYNAMIC INFLOW ON THE STABILITY OF ROTOR-BODY SYSTEMS

David A. Peters
Professor and Chairman
Department of Mechanical Engineering
Washington University
St. Louis, Missouri 63130

Abstract

The induced flow field of a rotor responds in a dynamic fashion to oscillations in rotor lift. This has long been known to affect the stability and control derivatives of the rotor. More recently, however, it has also been shown that this dynamic inflow also affects rotor and rotor-body aeroelastic stability. Thus, both the steady and unsteady inflow have pronounced effects on air resonance. Recent theoretical developments have been made in the modeling of dynamic inflow, and these have been verified experimentally. Thus, there is now a simple, verified dynamic inflow model for use in dynamic analyses.

Notation

a	=	slope of lift curve, per radian
B	=	tip loss factor
C_{do}	=	drag coefficient
C_{do}^*	=	equivalent drag coefficient
C_L	=	roll moment coefficient
C_M	=	pitch moment coefficient
C_Q	=	torque (or power) coefficient
C_T	=	thrust coefficient
e_{pc}	=	pocket cut-out divided by radius
$\{F\}$	=	vector of loadings
$\bar{f}$	=	flat plate drag area over rotor area
k	=	reduced frequency based on free stream, $= \omega/v$
K_I	=	apparent inertia coefficient
K_M	=	apparent mass coefficient
$[L]$	=	matrix of inflow gains
$[\mathcal{L}]$	=	normalized L matrix
$[M]$	=	inflow apparent mass matrix
p	=	nondimensional flapping frequency
r	=	nondimensional distance from rotor center, $0 < r < 1$
R_e	=	elastic coupling parameter
v	=	mass flow parameter
$\bar{v}$	=	nondimensional free stream
V_T	=	total nondimensional flow at rotor, Table 3
α	=	pitch angle, angle of incidence, positive nose down
α^*	=	pitch angle at rotor, $\alpha^* = \sin^{-1}[(\lambda + \nu)/\mu)]$
γ	=	Lock number
γ^*	=	equivalent Lock number
υ	=	nondimensional free-stream velocity
υ^*	=	free-stream velocity at rotor, $\upsilon^* = \sqrt{\mu^2 + (\lambda + \nu)^2}$
δ	=	axis of minimum damping
η	=	inplane damping
θ	=	total pitch angle
θ_o	=	collective pitch
θ_s, θ_c	=	cyclic pitch
λ	=	normal freestream component, $\lambda = \upsilon\sin\alpha$
λ_o	=	total uniform inflow, $\lambda_o = \lambda + \bar{\nu}$
λ_c	=	fore-to-aft steady gradient
μ	=	advance ratio, $\mu = \upsilon\cos\alpha$
ν	=	total induced flow
ν_o	=	uniform induced flow
ν_s	=	side-to-side induced flow gradient
ν_c	=	fore-to-aft induced flow gradient
ξ	=	axis along free stream
σ	=	rotor solidity, real part of eigenvalue

ORIGINAL PAGE IS
OF POOR QUALITY

ORIGINAL PAGE IS
OF POOR QUALITY

$[\tau]$ = matrix of inflow time constants

ϕ = inflow angle

ϕ_s = side-to-side gradient in inflow angle

ω = excitation frequency, imaginary part of eigenvalue, per rev

ω_ζ = inplane frequency, per rev

Ω = rotor speed, rpm

$\bar{(\ )}$ = average value

$\tilde{(\ )}$ = perturbation value

Introduction

Almost everyone would agree that the induced flow field of a rotor is an important contributor to the performance and vibrational characteristics of that rotor. What is less well known, however, is that the induced flow field of a rotor is also an important contributor to the aeromechanical stability of that rotor. The contribution of induced flow to stability is manifested in two ways. First, the steady induced-flow field affects the equilibrium flapping angles, the cyclic pitch, and the inflow angles of the rotor. These, in turn, impact directly upon aeromechanical stability. Second, the induced flow field responds (in a dynamic fashion) to oscillations of the rotor; and this inflow response can fundamentally change the damping of the rotor oscillation. Because of the important influence of unsteady induced flow, a good deal of effort has gone into the modeling of dynamic inflow for helicopter applications. This paper examines the history of this modeling effort including the latest developments and experimental verification.

Steady Inflow

The major contribution of steady inflow to rotor damping can be understood in terms of the axis of minimum damping, as shown in Figure 1. In the top figure, we see an airfoil pitched at an angle θ with the relative air flow impinging at an angle ϕ. The vertical direction is flap and the inplane direction is lead-lag. It turns out that the least stable direction of motion is at $(\theta + \phi)/2$, Reference 1. In other words, a coupled flap-lag mode with a principle direction of motion at $(\theta + \phi)/2$ will have the least damping of all modes. The physical basis for this "minimum damping" is illustrated in the lower part of the figure. The blade lift is always perpendicular to the direction of air flow. Thus, a blade motion directed along an axis δ creates an increased lift which is opposite to the direction of motion-damping. However, if δ is larger than ϕ, then lift is in the same direction as the motion and can create negative damping. The maximum negative contribution occurs at $\delta = (\theta + \phi)/2$.

Now, it is clear that the induced flow directly affects the angle ϕ. Thus, induced flow can either move the axis of minimum damping closer to the modal axis (which is destabilizing) or further from the modal axis (which is stabilizing).

The mathematical description of this phenomenon is given by

$$\eta = \eta_o + \left[\frac{\theta + \phi}{2} - \frac{R_e(\omega_\zeta^2 - p^2 + 1)}{(\omega_\zeta^2 - p^2)}\right]^2 \quad (1)$$

The negative real portion of the inplane eigenvalue is η and is a measure of inplane damping. Here, we see that there is a contribution to this damping that is minimum when $(\theta + \phi)/2$ is equal to the direction of blade motion. The modal direction depends upon the elastic coupling (R_e) and upon the difference between the inplane and flapping stiffnesses ($\omega_\zeta^2 - p^2$). For a stiff inplane rotor, $\omega_\zeta^2 > p^2$, the worst case is at a positive $\theta + \phi$. For soft inplane rotors, $p^2 - 1 < \omega_\zeta^2 < p^2$ (including those with matched-stiffness $\omega_\zeta^2 = p^2 - 1$), the worst case is for $\theta + \phi$ negative. This occurs during autorotational descent and partially accounts for the fact that autorotation is often the most critical air-resonance condition.

The effect of induced flow on inplane damping turns out to be the most powerful effect that forward flight exerts on inplane damping. To be more specific, the decrease in induced flow (that accompanies forward speed) and the tip-path tilt (that is used for propulsive force) both combine to significantly change the inflow as a function of μ. Figure 2, taken from Reference 2, depicts inplane damping as a function of advance ratio. The figure shows a sharp drop in damping with μ. When the μ-related changes in induced flow are ignored, however, as shown in the top curve, this loss of damping is not predicted. Therefore, we conclude that the major effect of advance ratio is the drop in ϕ (and hence the movement of the axis of minimum damping). In fact, up to $\mu = .25$, most of the effect of forward flight can be included by a hover analysis with inflow appropriately changed to account for forward flight. When propulsive trim is included (the short-dashed curve), the rotor shaft tilts forward with advance ratio to overcome fuselage drag. This tends to increase inflow and, therefore, to cancel the lower induced flow. Thus, for $\mu > .25$ the damping again increases.

ORIGINAL PAGE IS
OF POOR QUALITY

A similar phenomenon is manifested in wind turbine (or autorotatinal) damping, as shown in Figure 3, taken from Reference 3. Here, the wind-speed ratio directly affects ϕ, which results in minimum damping at a particular velocity. The same can be said of wind-turbine damping versus power coefficient, as seen in Figure 4. At a particular value of C_Q, the induced flow is such as to make the damping a minimum.

Thus far, we have considered only the uniform (or average) value of induced flow. It is also interesting to investigate the effect of gradients in the induced flow field. The Figure 5 compares inplane damping for the case of no gradients ($\lambda_c = 0$) with that for the case of a full gradient ($\lambda_c = \lambda_o$), which implies zero induced flow at the leading edge of the rotor disc and maximum induced flow at the trailing edge. One can see that there is only a minor variation in damping between the two cases. Even in hover (for which no gradient physically exists), the effect is small. Thus, fore-to-aft gradients are not important in the context of the effect of steady induced flow on inplane damping.

In Figure 6, we see the effect of a side-to-side gradient on inplane damping. A wind turbine is chosen, for which such gradients occur due to the earth's boundary layer. Here, there is some effect on stability at moderate μ. The reason for this is straight-forward. Changes in ψ from fore-to-aft generally cancel in terms of damping. Side-to-side gradients, on the other hand, tend not to cancel due to the large changes in relative free-stream velocity in forward flight. Thus, induced flow gradients are more important in the lateral direction than in the longitudinal; but neither effect is very large.

Early Work In Dynamic Inflow

In the preceding development, we have seen that the steady induced-flow field has a significant effect on blade damping. We now turn our attention to the effect of unsteady fluctuations in the flow field (dynamic inflow). To begin, it might be good to review the past developments in this area. In 1950, Ken Amer noted that the pitch-rate damping of a helicopter depends upon the thrust coefficient in a repeatable, quantitative fashion, Reference 4. In 1952, G. J. Sissingh successfully showed that this measured effect is due to a transient behavior of the induced flow, Reference 5. That is, a roll-rate of a helicopter causes a side-to-side gradient in lift which creates roll damping. However, the formation of this lift gradient also creates an induced-flow gradient that partially negates the lift gradient that finally develops. (This is the effect of dynamic inflow.) Since the induced flow depends greatly upon the mass flow through the rotor, there is a strong C_T dependence, as measured by Amer. In related work, Reference 6, Carpenter and Fridovitch developed experimental and theoretical results that related to how quickly induced flow follows a change in lift (i.e., a time constant). They found that the time delay could be modeled satisfactorily by the apparent mass of an impermeable disk, as developed in Reference 7. Therefore, by 1953, researchers had identified both the effect of transient inflow and the effect of apparent mass. These two pieces (the induced flow due to lift perturbations and the related time constants) form the kernel of all subsequent work in dynamic inflow.

The early work of these researchers was picked up by several investigators in the early 1970's. This later work concentrates on stability and control derivatives as well as forced response (both of which are dramatically affected by the dynamic inflow phenomenon identified by Sissingh). In 1970, Pat Curtiss and Norm Shupe included the Sissingh model in their helicopter flight equations, References 8-9. (This was a quasi-steady model, and no time constants were used.) The work of Curtiss and Shupe points out that the quasi-steady effect of induced flow in pitch and roll can be accounted for by a simple reduction in the lift coefficient (i.e., by an equivalent Lock number). In other words, changes in lift produce changes in inflow which lower the expected change in lift. Thus, we have an equivalently lower lift-curve slope and lower gamma.

In 1972, Ormiston and Peters took the Sissingh-Shupe model and extended it to include plunge, pitch, and roll for combinations of lift, climb, and forward flight, Reference 10. Calculations of control derivatives with this model were then compared with experimental data taken by Dave Sharpe and Bill Kusczynski with a 7-1/2 ft diameter model rotor. The results show that the Sissingh-Shupe dynamic inflow model (based on momentum theory) gives excellent correlation in hover but not in forward flight. Alternative models for forward flight were then suggested, including an empirical model based on curve fitting the measured data.

By 1974, Peters and Ormiston had extended the dynamic inflow models to the unsteady condition (time constants, etc), Reference 11. Sharpe and Kuczynski had obtained experimental frequency-response data both in hover and forward flight, Reference 12; and this data was compared to the theory in Reference 11. At the same time, Hohenemser and Crews were obtaining similar frequency-response data for a very small-scale rotor, Reference 13; and they also compared with theory. Both studies showed a dramatic effect of dynamic inflow. Furthermore, these two independent studies revealed a completely consistent picture of the gains and time constants of dynamic inflow. In hover, they found that momentum theory (combined with the apparent mass of an impermeable disc) captured all of the experimental features. Thus, when these theoretical gains and time constants were combined with the theory, amazing correlation was obtained.

ORIGINAL PAGE IS
OF POOR QUALITY

Figure 7 shows an example of this correlation. Here we have the roll moment (on the left) and the pitch moment (on the right) due to an oscillation in θ_s (longitudinal cyclic). Both the amplitude and the phase of the response are given. The circles are experimental data from the 7-1/2 ft rotor. The solid line is the normal theory in which only steady induced flow is taken (no dynamic inflow). The results are presented for frequencies of swashplate oscillation from 0 to 1.2 per revolution and for 4° of steady collective pitch. One notices large, qualitative deviations between the solid, theoretical curve and the experiment, especially in the phase of C_L and in the amplitude of C_M. The discrepancies are largest at small values of ω and decrease for larger values of ω. Perhaps the most significant aspect of the comparison (between the solid line and the data) is the fact that none of our standard analytic excuses could explain the difference. Collective pitch is only 4°, so there is no stall; and the analysis includes several elastic modes in flapping, so that the dynamics are well represented. Thus, the only candidate to improve correlation is dynamic inflow.

The short-dashed curve gives results for a simple, quasi-steady momentum-theory model of dynamic inflow. That is, the dynamic inflow is assumed to follow changes in lift immediately according to simple momentum theory. The result is dramatic. Every single detail of the data is matched for $\omega \leq .4$ per rev. At larger ω, however, the theory with quasi-steady theory begins to deviate from the experimental result. The reason for this is that inflow actually responds with a time delay. When this unsteady effect is added, however, (the long dashed curve) the new analysis agress at both low and high ω. The time constants used in this amazing correlation are the apparent mass and inertia of an impermeable disc. This yields the nondimensional inertia and mass terms ($K_I = .1132$, $K_m = .8488$). This simple theory leads to the correlation shown in both magnitude and phase.

It seems impossible that anyone could study these results and not be convinced that: a) dynamic inflow is an important, physically-based effect, and b) it can be modeled in hover by simple momentum theory with simple apparent mass terms. In general, one would not always admit that a theory is good simply because in improves correlation. In many cases, improvement might simply be luck; because there can be so <u>many</u> unknown effects that one error might coincidentally cancel another. In this case, however, all reasonable errors have been accounted for. Furthermore, the details of the response are so well simulated that coincidence is out of the question. These results establish dynamic inflow as a fundamental cornerstone of rotor analysis.

We now turn from the response of cyclic pitch oscillations and study the response due to shaft oscillations, as shown in Figure 8. Here, we look at the amplitude and phase of roll moment and pitch moment as a result of pitch oscillations. Because of the symmetry in hover, roll oscillations should create responses identical to those due to pitch (except for a 90° phase shift). Thus, both pitch and roll data are plotted together on this figure (circles and dots). Where the two sets of data begin to deviate ($\omega = .25$), a stand resonance is contaminating the results. Below $\omega = .25$, however, the pitch and roll data are consistent. The solid curve represents conventional theory with no dynamic inflow. One is impressed with how poorly it models the response. (C_L with α is in error by several hundred percent.) When either quasi-steady or unsteady dynamic inflow is included, however, the amplitude and the phase are completely captured. This data correlation leads one to believe that an air resonance mode could be very sensitive to dynamic inflow, since such modes occur from 0.2 to 0.5 per rev.

In forward flight, there is also a large effect of dynamic inflow; but it is not well modeled by simple momentum theory. Figure 9 shows response of the same rotor as that of the previous figures, but with $\mu = .51$. C_L due to all three controls is given. Momentum theory (shown by the dashed line) does not at all correlate with the data. The long dashed curve in the figure is a calculation based on an empirically identified model. This model is identified at <u>$\omega = 0$ only</u>. The effect of ω is included by the same apparent mass terms used in hover. Thus, we see an excellent correlation which includes the presence of an anti-resonance (zero amplitude and phase discontinuity) predicted and measured for the θ_s derivative at $\omega = .4$. Thus, dynamic inflow is important even at high advance ratios.

The effect of dynamic inflow and the satisfying correlation shown above are not flukes of one rotor in one wind tunnel. Figure 10 shows data taken by Kurt Hohenemser and Sam Crews with a 20-inch diameter rotor at Washington University, Reference 13. Here, harmonic excitation is applied in the rotating system by a rotating eccentric. The magnitude of flapping angle due to θ is plotted versus the excitation frequency in the rotating system, ω. The squares are the test data, the solid curve is the analysis with no dynamic inflow, and the dashed curve is the analysis including dynamic inflow. The parameters L and τ are chosen to give the best fit of the data, and yet they agree with the values from momentum theory within a few percent. For example, $K_I = .113$ (momentum), $K_I = .112$ (Reference 13). Therefore, dynamic inflow is established as an effect independent of rotor site or wind-tunnel characteristics.

ORIGINAL PAGE IS
OF POOR QUALITY

In summary, the early work in dynamic inflow concentrates on forced response of rotors. It shows beyond reasonable doubt that dynamic inflow is an important effect. In hover, the quasi-steady inflow is well modeled by momentum theory; but, in forward flight, momentum theory is completely inadequate. In both hover and forward flight, however, the apparent mass of an impermeable disc provides the correct time constants.

Effect On Stability

The superb data correlations given thus far were developed for the forced response of rotors. It was not long, however, before researchers began studying the effect that dynamic inflow might have on the stability and damping of rotor systems. We now mention a few of the developments in this area. In 1976, Bob Ormiston studied the effect on flapping eigenvalues, Reference 14. He discovered the importance of mode type (collective, progressing, regressing) on the effect of dynamic inflow. In 1979, Peters and Gaonkar studied the effect on lead-lag eigenvalues, Reference 15. One of the more interesting aspects of that paper was the introduction of an equivalent drag coefficient. In other words, just as the lowered lift (due to dynamic inflow) can be modeled by a loss in lift-curve slope, even so, the corresponding increase in induced drag (also caused by dynamic inflow) can be modeled by an equivalent increase in C_{d_o}.

In 1982, Gaonkar and several co-authors extended this work to include aeromechanical stability, Reference 16. That same year, Wayne Johnson also used dynamic inflow theory to correlate Bill Bousman's test data, Reference 17. At this point, it might be good to briefly review the findings of each of these papers with respect to the stability and damping of rotors.

First we look, in Figure 11, at the calculation from Reference 14 of the negative real part of the flapping eigenvalue as a function of collective pitch for $p = 1.02$ and 1.15. With no dynamic inflow, there is a constant value of damping equal to $\gamma/16$, independent of θ_o. When dynamic inflow is included in the analysis, however, one finds two distinct damping values depending upon the mode, progressing or regressing (collective is not included). The difference in damping of the two modes is attributed to the fact that each mode has a different frequency and therefore affects the inflow in a different way. The quasi-steady approximation (shown by the dashed curve) is closer to the regressing mode because that mode is of lower frequency. The results show clearly the large effect of dynamic inflow. The effect is most pronounced for the regressing mode at low collective pitch. Such a plot indicates that one cannot count on flap damping to stabilize ground resonance at low θ_o.

Another interesting aspect is that even the progressing mode, with a relatively high frequency, is affected by dynamic inflow.

Figure 12 shows the real part of the inplane eigenvalue as a function of advance ratio, Reference 15. The solid curve is the theory without dynamic inflow, and the broken curves are the modes with dynamic inflow. We notice that the higher-frequency progressing and collective modes are only moderately affected. The lower-frequency, regressing mode, however, shows a substantial alteration due to dynamic inflow. Thus, we conclude that dynamic inflow has a potentially large effect on inplane damping, and thus on rotor-body damping.

Next we look at calculations of coupled rotor-body modes from Reference 16, as shown in Figure 13. Here we have body roll-mode damping both for an RPM sweep and for a collective-pitch sweep. The dashed-dot curves are quasi-steady theory; and the dashed-only curves are conventional, unsteady theory. The rotor is matched stiffness. The figure on the left shows a fairly uniform effect of dynamic inflow within the RPM range of interest. This effect is about 30%. The right-hand figure gives a collective sweep. As might be expected, the effect of dynamic inflow increases with decreased lift. Again, the theoretical predictions are that dynamic inflow should play a major role in rotor-body damping; and this effect comes from equivalent changes in both flap damping and inplane damping, as we understand from Reference 16.

It fell to Wayne Johnson to finally compare these predictions with experimental data, as shown in Figure 14. This figure presents the real part of the eigenvalue for the pitch-mode damping. The dashed curve is the theory without inflow dynamics, and the solid curve is the theory with inflow dynamics. Dynamic inflow successfully predicts the peak in damping at low Ω and the 25-30% loss of damping at higher values of Ω. Figure 15 shows a similar comparison for roll. Again, the dynamic inflow provides a substantial improvement in correlation.

The previous two figures show that the NASA analytic model does reasonably well in correlation and that dynamic inflow is an important part of that correlation. Therefore, an analysis without dynamic inflow, but that correlated with experimental data, would be suspect, since dynamic inflow is well-documented and damping analyses are not, and since we know that dynamic inflow has an important effect.

For those who might still be skeptical, we present Figure 16, also from Reference 17. This figure compares measured and calculated frequencies as a function of RPM. The astounding part of the comparison is that one of the branches, labeled λ, is the frequency of a mode that is predominantly dynamic inflow. This branch does not even exist when dynamic inflow is not included. With dynamic inflow, however, the branch appears and matches the experimental data nearly perfectly. Thus, we are looking not just at the effect of dynamic inflow on some mode; we are looking at

the measured dynamic-inflow mode, itself, as seen for the first time.

A final comparison with data is given in Figure 17, which represents two of the correlation studies presented at this workshop. One is Wayne Johnson's correlation with the NASA program, and the other is Sheng Yin's correlation with the Bell Helicopter program. In either case, dynamic inflow represents a significant contribution and improves the correlation of the analysis.

Before leaving the stability correlation, we need to make an important point about the role of these correlations in verifying dynamic inflow theories. The point is this. The validity of a particular dynamic inflow theory (or of dynamic inflow as a phenomenon) cannot presently be made on the basis of comparisons with inplane damping or rotor-body stability data. The reason for this is clear. Stability calculations are not yet accurate enough to uniquely distinguish dynamic inflow from other effects. The role of dynamic inflow in such calculations is, however, important. The reason for this is straightforward. First, we know from flapping response that dynamic inflow exists as a phenomenon and that it is important. The accuracy of any dynamic inflow theory can be determined by comparisons with low-lift flapping response data, which is accurate and relatively unhindered by unknown structural or aerodynamic effects. It is this exact same theory that is applied to inplane stability analyses. (There is not one "flapping" dynamic inflow and one "inplane" dynamic inflow.) Therefore, the comparison with stability data does not test the inflow theory. Instead, the dynamic inflow theory is included in the analysis in order to see the effect of dynamic inflow and to verify the analysis package. This is why we said earlier that a theory that correlates without dynamic inflow would be suspect. Such a theory must have two errors that are cancelling. One error is the omission of dynamic inflow, and the other error is the unknown omission that is somehow cancelling the inflow effect.

Momentum-Theory Formulation

In the early portions of this paper, we briefly reviewed the early work in dynamic inflow; but we did not go into detail as to the exact mathematical formulations used. In this section, we consider these formulations in more detail. The vast majority of the work in this area has been based on simple momentum theory. In hover, this implies that each elemental section of rotor area is treated independently. Then, for each section, the thrust is set equal to the product of the mass flow through the element and the total change in velocity in the associated stream tube. The next step in the analysis (and this is crucial to the theory) is to average the loads and induced flow over the rotor disc. In other words, the theory of dynamic inflow does not concern itself with details of either load distribution or induced flow distribution. It concerns itself, rather, with global averages. This further implies that the induced flow is treated more as a large mass of air rather than as individual vortices.

As a simple example, we consider the average induced flow ν due to the total thrust coefficient, C_T

$$C_T = 2\nu^2 \tag{2}$$

Equation (2) is nonlinear in ν. Usually, however, we consider perturbations about a steady condition $(\bar{C}_T, \bar{\nu})$. Thus, we have for the quasi-steady case

$$C_T = \bar{C}_T + \tilde{C}_T \tag{3a}$$

$$\nu = \bar{\nu} + \nu_o \tag{3b}$$

$$\bar{C}_T = 2\bar{\nu}^2 \tag{4a}$$

$$\tilde{C}_T = 4\bar{\nu}\nu_o \tag{4b}$$

Equation (4b) is the typical perturbation relation between charges in thrust, C_T, and charges in uniform inflow, ν_o. In a more general formulation, we may add cyclic variations in lift (i.e. roll and pitch moments) and cyclic variations in induced flow

$$\nu = \bar{\nu} + \tilde{\nu} \tag{5a}$$

$$\tilde{\nu} = \nu_o + \nu_s r\sin\psi + \nu_c r\cos\psi \tag{5b}$$

where ν_s and ν_c are induced flow gradients. Simple momentum theory gives

$$\tilde{C}_T = 4\bar{\nu}\nu_o \tag{6a}$$

$$\tilde{C}_L = -\bar{\nu}\nu_s \tag{6b}$$

$$\tilde{C}_M = -\bar{\nu}\nu_c \tag{6c}$$

Equations (6a-c) represent the momentum theory model in hover used in References 5, 8, 9, 10, 11, 14, 15, and 16.

Although equation (6) works well for hover, it is natural to try to extend the formulation to combinations of thrust, climb, and forward flight. To do this, $\bar{\nu}$ in equations (6a-c) is replaced by $v/2$ where v is a mass-flow parameter. In climb,

ORIGINAL PAGE IS
OF POOR QUALITY

ORIGINAL PAGE IS
OF POOR QUALITY

v is given by

$$v = \lambda + 2\bar{v} = \lambda_o + \bar{v} \tag{7}$$

where λ is the inflow due to climb, and λ_o is the total inflow, Reference 8. In forward flight with perfectly edgewise flow and no lift, we have

$$v = \mu \tag{8}$$

as given in Reference 9 and 10, (although forward flight certainly stretches the assumptions of momentum theory to the extreme).

Most investigators agree on the formulations of equations (7) and (8), but a more difficult problem is the transition from hover to edgewise flow. If we consider a freestream velocity υ and a rotor incidence α, then the relative flow is given by

$$\mu = \upsilon \cos \alpha \tag{9a}$$

$$\lambda = \upsilon \sin \alpha \tag{9b}$$

$$\upsilon = \sqrt{\mu^2 + \lambda^2} \tag{9c}$$

If we then add the induced flow, we obtain for the flow at the rotor disc

$$\lambda_o = \upsilon \sin\alpha + \bar{v} = \lambda + \bar{v} \tag{10a}$$

$$\upsilon^* = \sqrt{\mu^2 + (\lambda + \bar{v})^2} = \sqrt{\mu^2 + \lambda_o^2} \tag{10b}$$

$$\alpha^* = \tan^{-1}\left(\frac{\lambda + \bar{v}}{\mu}\right) = \tan^{-1}\left(\frac{\lambda_o}{\mu}\right) \tag{10c}$$

The real problem is to relate v to μ, λ, and $\bar{v}$.

In References 9 and 18, this is accomplished by the following ad hoc formula

$$v = \upsilon + 2\bar{v} \sin \alpha = \frac{\mu^2 + \lambda^2 + 2\bar{v}}{\sqrt{\mu^2 + \lambda^2}} \tag{11}$$

Equation (11) gives the correct value of v in hover ($\mu = 0$, $v = \lambda + 2\bar{v}$); but for edgewise flow, equation (11) gives an inconsistent result ($\lambda = 0$, $v = \mu$). Now, $v = \mu$ is correct for edgewise flow with no lift; but the inconsistency is that, for $\lambda = 0$, equation (11) gives no effect of thrust (i.e. of $\bar{v}$) in the formula. Thus, in the limit as ($\lambda = 0, \mu \to 0$) we obtain a different value of v than we do for ($\mu = 0$, $\lambda \to 0$). There is a discontinuity in the function at ($\mu = 0$, $\lambda = 0$), and this is unacceptable.

A more reasonable formulation of v is given in Reference 11 from basic principles

$$v = \upsilon^* + \bar{v} \sin \alpha^* = \frac{\mu^2 + (\lambda + \bar{v})(\lambda + 2\bar{v})}{\sqrt{\mu^2 + (\lambda + \bar{v})^2}} \tag{12}$$

where υ^* and α^* are the total flow and angle at the rotor including induced flow. Equation (12) is derived from momentum principles (not on an ad hoc basis) and provides a much more reasonable formulation of the transition between hover and forward flight. When v is represented by equation (12), it is always positive (with no singularities) except at the vortex-ring boundary, where $v = 0$, Reference 19.

In more recent work by Johnson, Reference 20, equation (12) is obtained for the C_T relation, equation (6a); but a different formulation is derived for the C_L and C_M relations, equations (6b) and (6c). In particular, Reference 20 uses for C_L and C_M

$$v = \upsilon^* = \sqrt{\mu^2 + (\lambda + \bar{v})^2} \tag{13}$$

This is in direct contrast to equation (12). Furthermore, in Reference (20), the v for the C_T relation is altered by use of an "approximation" of equation (12)

$$v = \upsilon^* + \upsilon \sin\alpha^* \simeq \upsilon^* + \lambda + \bar{v} = \sqrt{\mu^2 + (\lambda + \bar{v})^2} + (\lambda + \bar{v}) \tag{14}$$

It is not at all clear why the approximation in equation (14) should be valid. Although Reference (20) states that it is valid "for low inflow ratio," this claim is actually not correct.

Table 1 provides a comparison of equations (11)-(14) at critical flight conditions. There are several interesting comparisons in the table. First, in the hover results, we note the Johnson model for roll and pitch differs by a factor of 2 from all previous work (including Sissingh, Curtiss, Shupe, Ormiston, Peters, and Azuma), even in hover. Since these previous results show such an excellent correlation with flapping data, there can be little doubt that Reference 20 is in error. The source of the error can be quickly traced to a failure to include v_s and v_c in the mass flow term of each generic element. Along this same line, Reference 20 mentions agreement with the results of Loewy, Reference 21, as confirmation of the accuracy of the formulation. Reference 21, however, is for a zero-lift climb (no wake contraction). The second row of Table 1 shows that for a climb, equation (13) is acceptable for roll and pitch, giving the correct answer $v = \lambda$. With lift, however, the formulation is incorrect.

The second row of Table 1 also reveals an error in the C_T formulation of Reference 20. Whereas all other formulations (including Reference 21) result in $v = \lambda$, the approximation of equation (14) (from Reference 20) gives $v = 2\lambda$. Here, the error lies in the approximation and not in the original formulation. When the conditions of climb and lift are combined, the third row of Table 1, the error in the formulation of Reference 20 is more clear. The correct value, $\lambda + 2\bar{v}$, is the flow speed downstream from the rotor. The two incorrect formulas $(\lambda + \bar{v})$ and $2(\lambda + \bar{v})$ do not provide any effect of wake contraction, for they treat thrust and climb equally.

Going on with Table 1, we see that all formulations give the same value, $v = \mu$, for zero lift edgewise flow; but when lift is added, row 5, there is a wide range of answers. Only the results of Reference 11 and Reference 20 (C_T) are consistent in the sense that they reduce both to μ as $\bar{v} \to 0$ and to $2\bar{v}$ as $\mu \to 0$. When we further consider the case of zero lift but with incidence, row 6, the results of Reference 20 (C_T) also fail, which leaves the result of Reference 11 as the only viable choice. (For no lift, only $\sqrt{\mu^2 + \lambda^2}$ makes physical sense.) Finally, the last row of Table 1 gives results for zero normal flow, which can occur in a descent. Here, another failure of Reference 8 is noticed. Thus, the v parameter from Reference 11 is the most logical choice of transition between hover and forward flight in momentum theory. To summarize, its attributes are:

1) Correct limiting behavior in climb, hover, and edgewise flow

2) No singularities

3) Foundation in momentum theory

4) Prediction of vortex-ring boundary

The above discussion has considered only the quasi-steady effect of inflow. (Induced flow is assumed to follow immediately any change in loads.) The concept of momentum theory can also be extended, however, to include the time lag between lift and induced flow. In general, equations (6a-c) can be extended as follows.

$$K_M \dot{v}_o + 2v v_o = \tilde{C}_T \tag{15a}$$

$$K_I \dot{v}_s + v/2\, v_s = -\tilde{C}_L \tag{15b}$$

$$K_I \dot{v}_c + v/2\, v_c = -\tilde{C}_M \tag{15c}$$

Here K_M and K_I are time constants associated with the rotor air mass. These can be taken as completely general and identified experimentally, as in References 6 and 13. On the other hand, they can be obtained from first principles by potential flow theory. K_M is developed (in Reference 7) and K_I is found (in Reference 11) in this way.

$$K_M = \frac{8}{3\pi} = .8488 \tag{16a}$$

$$K_I = \frac{16}{45\pi} = .1132 \tag{16b}$$

In each case, the parameters are based on the apparent mass (or inertia) of an impermeable disc. Equations (15) and (16) form a complete unsteady dynamic inflow theory. With $K_M = K_I = 0$, we recover quasi-steady theory.

One of the most valuable results of momentum-theory inflow dynamics has been the discovery that the quasi-steady theory is tantamount to the use of an equivalent Lock number and drag coefficient, References 9 and 15. The formulation is as follows

$$\gamma^* = \frac{\gamma}{1 + \frac{\sigma a}{8v}} \tag{17a}$$

$$\left(\gamma \frac{C_{do}}{a}\right)^* = \gamma\left[\frac{C_{do}}{a} + \frac{(\theta - \phi)^2}{1 + 8v/\sigma a}\right] \tag{17b}$$

ORIGINAL PAGE IS
OF POOR QUALITY

$$\left(\frac{C_{do}}{a}\right)^{*} = \frac{C_{do}}{a}\left(1 + \frac{\sigma a}{8v}\right) + \frac{\sigma a}{8v}(\theta - \phi)^2 \qquad (17c)$$

Although equation (17a) was originally derived for rigid flapping only, Reference 22 shows that the formulation is quite general. Therefore, a simplified estimate of the effect of dynamic inflow can be obtained from a simple change of γ and C_{do} in any analysis package.

Another interesting aspect of the γ^{*} approximation is that it can also be used in unsteady, harmonic response analyses, Reference 11 and 13. In particular,

$$\frac{\gamma^{*}}{\gamma} = 1 - \frac{1}{1 + \frac{8v}{\sigma a} + \frac{16K_I i\omega}{\sigma a}} \qquad (18a)$$

The crucial parameter may be rewritten as

$$\frac{8v}{\sigma a} + \frac{16K_I i\omega}{\sigma a} = \frac{8v}{\sigma a}\left(1 + \frac{2i\omega K_I}{v}\right) \qquad (18b)$$

Equation (18b) shows that there is a reduced frequency, $k = \omega/v$, associated with dynamic inflow. Therefore, the effect of mass flow, v, can be very complicated since it changes both gain and reduced frequency.

More Advanced Formulations

The formulation of equations (15a-c), while being excellent in hover, has proven very poor in forward flight. (For example, it does not allow for a fore-to-aft gradient due to C_T.) For this reason, several attempts have been made to extend the theory. Up to now, all such attempts have been based on a matrix formulation of equation (15).

$$[\tau]\begin{Bmatrix}\dot{\nu}_o\\ \dot{\nu}_s\\ \dot{\nu}_c\end{Bmatrix} + \begin{Bmatrix}\nu_o\\ \nu_s\\ \nu_c\end{Bmatrix} = [L]\begin{Bmatrix}\tilde{C}_T\\ \tilde{C}_L\\ \tilde{C}_M\end{Bmatrix} \qquad (19a)$$

$$[M]\begin{Bmatrix}\dot{\nu}_o\\ \dot{\nu}_s\\ \dot{\nu}_c\end{Bmatrix} + [L]^{-1}\begin{Bmatrix}\nu_o\\ \nu_s\\ \nu_c\end{Bmatrix} = \begin{Bmatrix}\tilde{C}_T\\ \tilde{C}_L\\ \tilde{C}_M\end{Bmatrix} \qquad (19b)$$

$$[M]\{\dot{\nu}\} + [L]^{-1}\{\nu\} = \{F\} \qquad (19c)$$

If we look at equation (19a) and temporarily ignore the "dot" term, we see a quasi-steady inflow law. The various harmonics of inflow (described by a vector, $\{\nu\}$) are assumed to be linearly proportional to the aerodynamic loads on the blade (such as thrust, roll moment, and pitch moment). These loads are represented by the vector, F. The matrix L is the dynamic inflow matrix and expresses the coupling relationships between inflow and loads. Generally, we consider $\{\nu\}$ and $\{F\}$ in this equation to be perturbation quantities about some steady inflow and loading distributions.

The term, $[\tau]\{\dot{\nu}\}$, then represents time constants of the system. These imply that the induced flow does not instantaneously follow perturbations to the loads. The τ-terms imply "unsteady" as opposed to "quasi-steady" inflow theory. In an equivalent form of the general theory, given by the second matrix equation, the system is premultiplied by L-inverse. In this alternative version, the $L^{-1}\tau$ matrix takes on the roll of apparent mass terms, [M]. The crux of all dynamic inflow theories is to find the elements of L and [M]. In the early momentum theory (Sissingh, Curtis, Shupe, and Peters), the M-matrix and the L-matrix were diagonal, 3 x 3 matrices, as given by equation (15). In later work, Reference 10, other [L] matrices were considered based on empirical considerations. These were very successful, but lacked physical foundation. Thus, a need was recognized to find [L] and [M] from more basic theories.

In principle, any induced flow theory that keeps track of the three-dimensional, unsteady vorticity automatically includes dynamic inflow, e.g., Reference 21. In practice, however, few present-day programs provide a transient rotor wake analysis. Furthermore, even the steady wake programs are much too cumbersome for use in a dynamics analysis, Reference 23. What is needed, therefore, is some analysis that can be used to obtain [M] and [L] in a simple, usable form. The prime candidate for this analysis is actuator-disc theory. In Reference 24, the first attempt was made to extract dynamic inflow data from an actuator-disc theory. It should be pointed out that many people had used actuator-disc theories to obtain induced flow, but no one had exercised them in the context of obtaining dynamic-inflow derivatives.

Although Reference 23 came a long way toward the desired answer, the analysis became so involved that no definitive results could be obtained. The problem is illustrated by Figure 18. The dynamic inflow theory is just one part of an overall rotor analysis. However, if one tries to identify the inflow law in the presence of blade dynamics and airfoil theories, the problem becomes too complicated for a fundamental solution. What is needed is a look at the open-loop transfer function of dynamic inflow without the complications of blade theory.

The ideal theory for attempting such a derivation is the actuator-disc theory of Mangler and Squire, as applied by Joglekar and Loewy in Reference 25. This theory is based on the Kinner closed-form pressure potentials for an actuator disc. Figure 19 gives a schematic of such a disc in an ellipsoidal coordinate system (ν,η,ψ). The free-stream enters at an angle α, and positive lift is taken in the negative Z direction. Kinner was able to obtain a closed-form potential function to describe an arbitrary pressure discontinuity across the disc. This function is expressed in terms of Legendre functions and can be used to find the induced-flow field for any given loading. Although the theory is successfully applied (in Reference 25) to give a specific inflow distribution, it is not used to find the dynamic inflow matrices.

In Reference 27, Dale Pitt extends the Kinner theory to include unsteady effects and uses it to find the elements of [L] and [M]. Two different radial lift distributions are used to verify that the matrices are not sensitive to the details of blade loading. Table 2 provides the final forms of the matrices as suggested in Reference 26, where [L] takes the form

$$[L] = \frac{1}{v} [\mathcal{L}] \qquad (20)$$

The $[\mathcal{L}]$ matrix is symmetric with elements that depend only upon the angle of incidence, α. The entire matrix is divided by the free-stream velocity, v. For forward flight with lift, v becomes the mass flow parameter of equation (12) and α becomes the local angle, α^*, equation (10c). In axial flow ($\alpha = \alpha^* = 90°$), the [L] matrix reduces to that of momentum theory, a very satisfying result of the theory. Similarly, the M-matrix also agrees with momentum theory for the roll and pitch inertias, although the apparent mass for thrust is different than that of momentum theory when the loading is zero at the rotor center.

In Reference 27, the formulation of Table 2 has been verified by two independent means. First, for the quasi-steady terms, the [L] matrix has been checked against a free-vortex wake analysis written by Landgrebe. The prescribed wake model of Landgrebe is exercised in numerical experiments in which changes in cyclic and collective pitch create changes in induced flow patterns, and these are interpreted in terms of the wake coupling matrix, L. Figure 20 presents the first column of L, inflow due to thrust. The horizontal line is the theoretical value of $L_{11} = 1/2$ that relates thrust to uniform inflow; it is completely independent of lift distribution. The open triangles are results from the wake program and agree within 10%. The long-dashed and dash-dot lines provide the L_{31} term, which is zero in hover ($\alpha = 90°$) and maximum at $\alpha = 0°$. Two different loading distributions are used, labelled "corrected" and "uncorrected." The results from Landgrebe's program are given by squares. (Solid squares indicate convergence problems.) The corrected curve, which enforces zero lift at the center, is very close to the Landgrebe results, and is the formulation used in Table 2. The two solid squares are suspect because no data has ever shown the fore-to-aft gradient decreasing as incidence goes to zero. The L_{21} term is zero for both the theory and the Landgrebe model.

Figure 21 provides a comparison of the second column of L, induced flow due to roll moment. In theory, the only term should be L_{22}, given by the two curves and the triangles. One can see that there is little difference in L_{22} for the two possible lift distributions. Furthermore, the prescribed-wake results agree to within a few percent for $\alpha > 30°$. Therefore, the simpler uncorrected curve is used in Table 2. L_{32} on the other hand (fore-to-aft inflow due to roll moment, shown by squares) is theoretically zero but exhibits a non-zero value from the prescribed wake. The explanation of this is the wake rotation (which is not included in the actuator-disc theory). Fortunately, the effect is not large. L_{12} is zero for both theory and numerical experiment.

When we look at the third column of L, Figure 22, we again see the wake rotation effect $L_{23} = -L_{32} = .2$, ideally zero from actuator-disc theory. The L_{33} term, shown as diamonds, displays an excellent correlation between actuator-disc and vortex models, as does the L_{13} term, shown in triangles. Again, the corrected versus uncorrected pressure distributions do not show an appreciable effect on L, and uncorrected is used in Table 2.

Reference 27 also provides a verification of the unsteady part of dynamic inflow, the M-matrix. In particular, an exact solution of the unsteady, potential flow equations is compared to the simpler approach of a direct superposition of $[L]^{-1}\{v\}$ and $[M]\{\dot{v}\}$ terms. The result is given in Figure 23 for $L_{22} = L_{33}$ ($\alpha = 90°$) as a function of reduced frequency, $k = \omega/v$. For both magnitude and phase, the simple model of equation (19) gives excellent agreement with a more rigorous, Theodersen-type, unsteady theory.

It should also be mentioned here that References 26 and 27 discuss the possibility of using additional radial and azimuthal degrees of freedom in the inflow model, and an expanded 5 x 5 model is explicitly given. In Reference 28, this 5 x 5 model is compared to the 3 x 3 model with respect to its effect on inplane damping. The results show two

ORIGINAL PAGE IS
OF POOR QUALITY

things. First of all, the 5 x 5 model gives extraneous answers for rotors with less than 5 blades (as a result of a mathematical indeterminancy). Second, for rotors with 5 or more blades (or for constant-coefficient analyses), the 5 x 5 results are essentially the same as the 3 x 3 results. Therefore, Reference 28 concludes that the 3 x 3 model is adequate and is probably the most sophisticated model that is possible for dynamic inflow in matrix formulation.

With dynamic inflow verified by both experimental and computational data, it is presently ready to be used in dynamics analyses. The theory as it now stands is a perturbation theory and thus applicable to linearized analysis packages. It is easily extended, however, to a nonlinear version for use in time history solutions. Table 3 shows the nonlinear version of L. Here, ν_o represents the total uniform induced flow (steady plus perturbation). You may recall that the linear version of L is divided by v, the mass-flow parameter, equation (20). In the nonlinear version, the first column of L is divided instead by the total mass flow V_T. The mass flow parameter v is simply related to V_T through a derivative as shown. Consequently, the nonlinear L-matrix has perturbation equations identical to those of the linearized dynamic-inflow theory.

Summary

The following statements summarize our present understanding of the importance of inflow to rotor and rotor-body damping.

1. Steady inflow (mostly uniform) is important for inplane damping in that it changes the axis of minimum damping.

2. The largest effect of advance ratio on inplane damping is the associate change in inflow.

3. Dynamic inflow is an important effect on rotor damping, and its importance has been physically verified many times.

4. The effect of dynamic inflow is largest for the low-frequency, regressing rotor-body modes.

5. Presently, the best dynamic-inflow theory is a 3 x 3 closed-form model based on actuator-disc theory. It's accuracy has been verified by comparisons with more sophisticated models.

References

1. Peters, David A., "An Approximate Closed-Form Solution for Lead-Lag Damping of Rotor Blades in Hover," NASA TM X-62,425, April 1975.

2. Peters, David A., "Flap-Lag Stability of Helicopter Rotor Blades in Forward Flight, "Journal of the American Helicopter Society, Vol. 20, No. 4, October 1975, pp. 2-13.

3. Wei, F-S and Peters, D. A., "Lag Damping in Autorotation by a Perturbation Method," Proceedings of the 34th Annual National Forum of the American Helicopter Society, Washington, D.C., May 1978, Paper 78-25.

4. Amer, K. B., "Theory of Helicopter Damping in Pitch or Roll and a Comparison with Flight Measurements," NACA TN-2136, October 1950.

5. Sissingh, G. J., "The Effect of Induced Velocity Variation on Helicopter Rotor Damping in Pitch or Roll," Aeronautical Research Council Paper No. 101, Technical Note No. Aero 2132, November 1952.

6. Carpenter, P. J. and Fridovitch, B., "Effect of Rapid Blade Pitch Increase on the Thrust and Induced Velocity Response of a Full Scale Helicopter Rotor," NACA TN-3044, November 1953.

7. Tuckerman, L. B., "Inertia Factors of Ellipsoids for Use in Airship Design," NACA Report No. 210, 1925.

8. Shupe, N. K., A Study of the Dynamic Motions of Hingeless Rotored Helicopters, Ph.D. Thesis, Princeton, September 1970.

9. Curtiss, H. C., Jr. and Shupe, N. K., "A Stability and Control Theory for Hingeless Rotors," Proceedings of the 27th Annual National Forum of the American Helicopter Society, May 1971, Paper No. 541.

10. Ormiston, Robert A. and Peters, David A., "Hingeless Rotor Response with Nonuniform Inflow and Elastic Blade Bending," Journal of Aircraft, Vol. 9, No. 10, October 1972, pp 730-736.

11. Peters, David A., "Hingeless Rotor Frequency Response with Unsteady Inflow," Rotorcraft Dynamics, NASA SP-352, February 1974I pp 1-13.

12. Kuczynski, W. A. and Sissingh, G. J., "Characteristics of Hingeless Rotors with Hub Moment Feedback Controls Including Experimental Rotor Frequency Response," NASA CR 114427, January 1972.

13. Crews, S. T., Hohenemser, K. H., and Ormiston, R. A., "An Unsteady Wake Model for a Hingeless Rotor," Journal of Aircraft, Vol. 10, No. 12, December 1973, pp 758-760.

14. Ormiston, Robert A., "Application of Simplified Inflow Models to Rotorcraft Dynamic Analysis," Journal of the American Helicopter Society, Vol. 21, No. 3, July 1976, pp 34-39.

15. Peters, David A. and Gaonkar, Gopal H., "Theoretical Flap-Lag Damping with Various Dynamic Inflow Models," Journal of the American Helicopter Society, Vol. 25, No. 3, July 1980, pp 29-36.

16. Gaonkar, G. H., Mitra, A. K., Reddy, T.S.R., and Peters, D. A., "Sensitivity of Helicopter Aeromechanical Stability to Dynamic Inflow," Vertica, Vol. 6, No. 1, January 1982, pp 59-75.

17. Johnson, Wayne, "Influence of Unsteady Aerodynamics on Hingeless Rotor Ground Resonance," Journal of Aircraft, Vol. 19, No. 8, August 1982, pp 668-673.

18. Azuma, Akira and Nakamura, Yoshiya, "Pitch Damping of Helicopter Rotor with Nonuniform Inflow," Journal of Aircraft, Vol. 11, No. 10, October 1974, pp 639-646.

19. Peters, D. A. and Chen, S. K., "Momentum Theory, Dynamic Inflow, and the Vortex Ring State," Journal of the American Helicopter Society, Vol. 27, No. 3, July 1982, pp 18-24.

20. Johnson, Wayne, Helicopter Theory, Princeton University Press, 1980, pp 520-526.

21. Loewy, R. G., "A Two-Dimensional Approximation to the Unsteady Aerodynamics of Rotary Wings," Journal of Aeronautical Sciences, Vol. 24, 1957.

22. Gaonkar, Mitra, and Reddy, "Feasibility of a Rotor Flight Dynamics Model with First-Order Cyclic Inflow and Multi-Blade Modes," proceedings of the AIAA Dynamics Specialists' Meeting, Atlanta, Georgia, April 9-10, 1981, p 15.

23. Landgrebe, A. J., "An Analytical Method for Predicting Rotor Wake Geometry," Journal of the American Helicopter Society, Vol. 14, No. 4, October 1969.

24. Ormiston, Robert A., "An Actuator Disc Theory for Rotor Wake Induced Velocities," AGARD Specialists Meeting on the Aerodynamics of Rotary Wings, Marseille, France, September 13-15, 1972.

25. Joglekar, M. and Loewy, R., "An Actuator-Disc Analysis of Helicopter Wake Geometry and the Corresponding Blade Response," USAAVLABLS Technical Report 09-66, 1970.

26. Pitt, Dale M. and Peters, David A., "Theoretical Predictions of Dynamic Inflow Derivatives," Vertica, Vol 5, No. 1, March 1981.

27. Pitt, Dale M. and Peters, David A., "Rotor Dynamic-Inflow Derivatives and Time Constants from Various Inflow Models, "9th European Rotorcraft Conference, Stresa, Italy, September 13-15, 1983, Paper No. 55.

28. Gaonkar, et. al., "The Use of Actuator-Disc Dynamic Inflow for Helicopter Flap-Lag Stability," Journal of the American Helicopter Society, Vol. 28, No. 3, July 1983, pp 79-88.

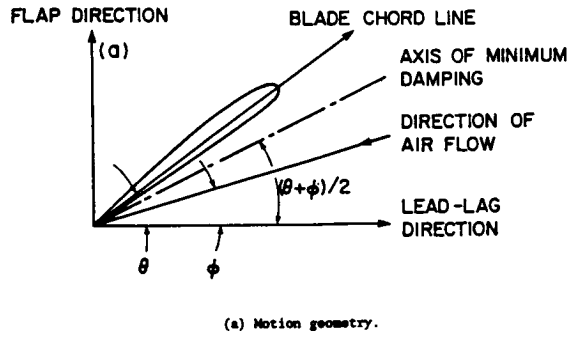

(a) Motion geometry.

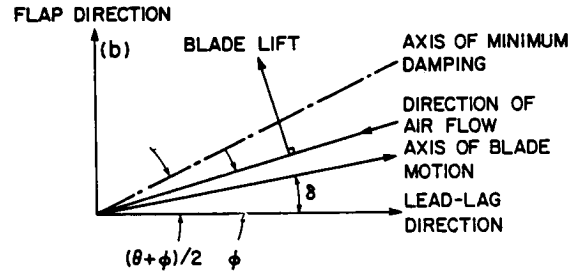

(b) Force geometry.

Figure 1. The Axis of Minimum Damping.

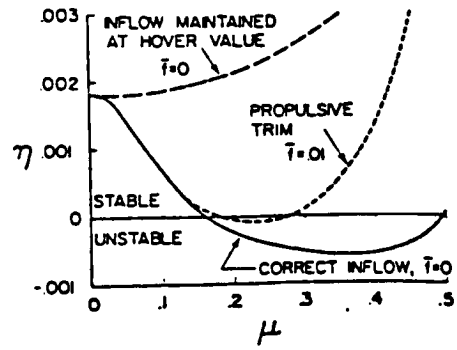

Figure 2. Effect of Inflow on Inplane Damping, p=1.15, ω_ζ=1.4, R_e=0, γ=5, σ=.05, C_{d_o}=0.1, C_T/σ=0.2, trimmed.

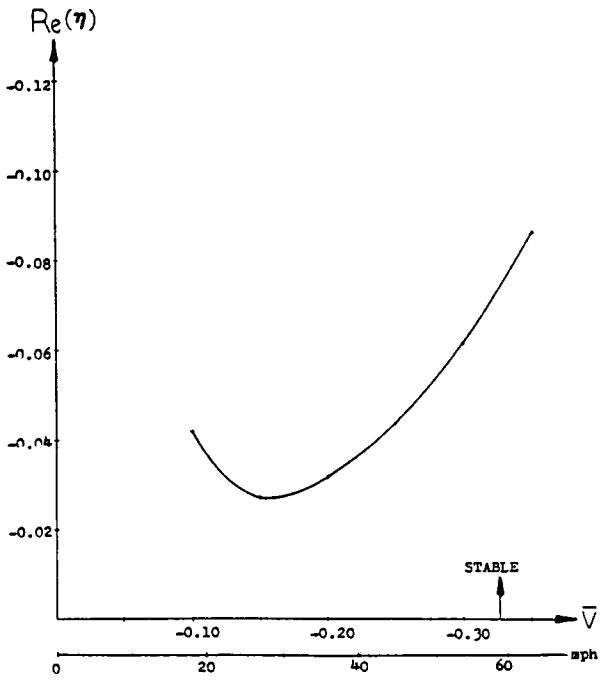

Figure 3. Wind Turbine Inplane Damping Versus Wind Speed, γ'=12.3, p=2.76, ω_ζ=3.62, C_{d_o}=.01, C_Q/σ=.007, σ=.0255, R_e=1.0, μ=0.0.

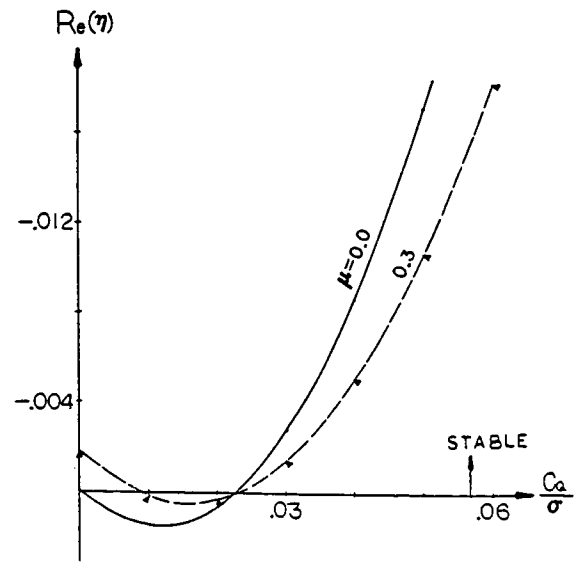

Figure 4. Wind Turbine Inplane Damping Versus Power Coefficients, C_T=.01, ω_ζ=0.7, R_e=0.0, $\bar{\sigma}$=.05, p=1.15, γ'=5.0, C_{d_o}=.01.

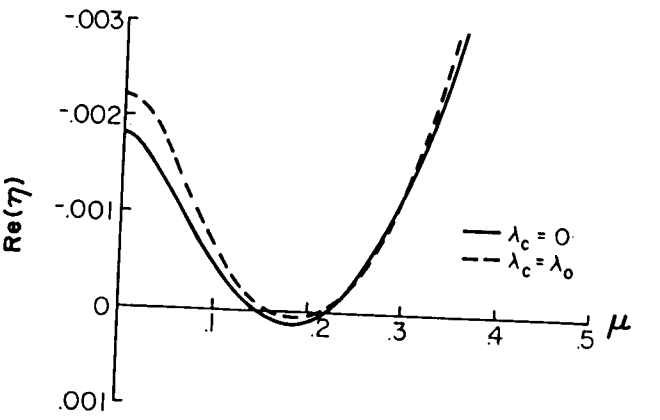

Figure 5. Effect of Fore-to-Aft Inflow Gradients on Inplane Damping, p=1.15, ω_ζ=1.4, R_e=0, γ'=5, $\bar{\sigma}$=.05, C_{d_o}=.01, ϵ_o=0.3, ϵ_s=ϵ_c=0.

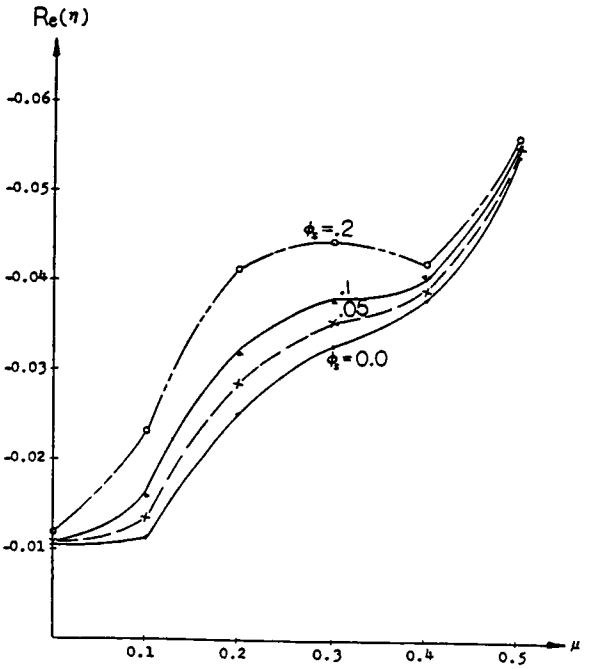

Figure 6. Effect of Lateral Gradients on Inplane Damping of Wind Turbine, C_T=.01, $C_Q/\bar{\sigma}$=.06, $\bar{\sigma}$=.05, p=1.15, ω_ζ=1.4, C_{d_o}=.01, γ'=5.0.

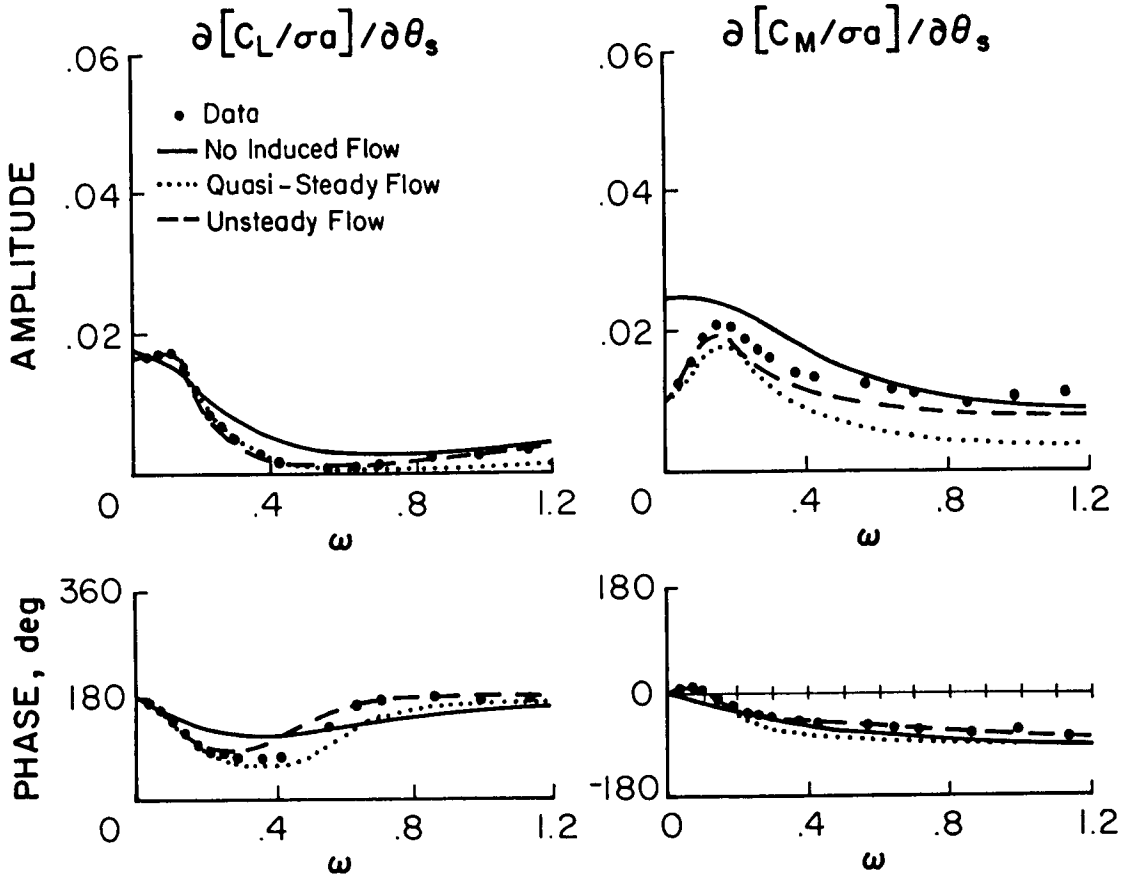

Figure 7. Rotor Response to Cyclic Pitch in Hover, p=1.15, γ=4.25, B=.97, e_{pc}=.25, μ=0, σa=.7294, $\bar{\nu}=\bar{\lambda}$=.03, θ_o=4°, momentum theory, single rotating mode.

ORIGINAL PAGE IS
OF POOR QUALITY

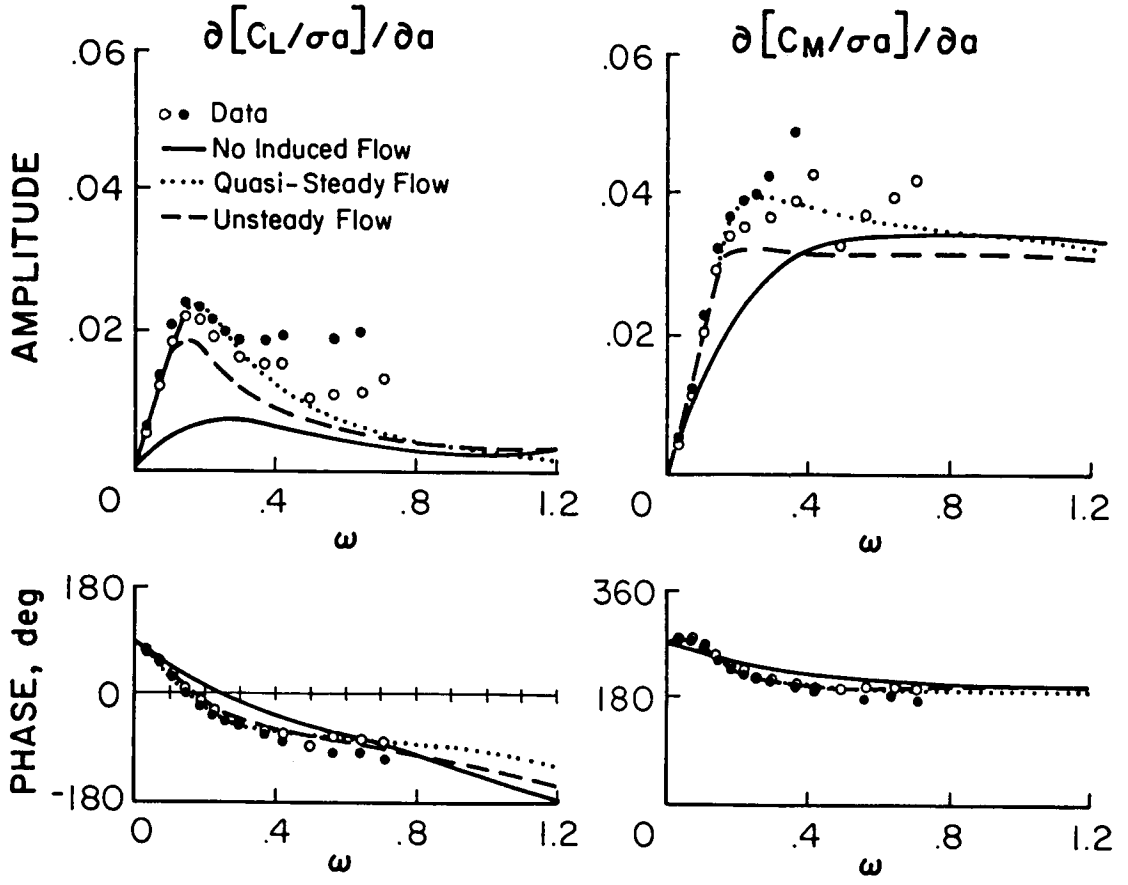

Figure 8. Rotor Response to Hub Motions in Hover, p=1.15, γ=4.25, B=.97, e_{pc}=.25, μ=0, σa=.7294, $\bar{\nu}=\bar{\lambda}$=.03, Θ_o=4°, momentum theory, single rotating mode.

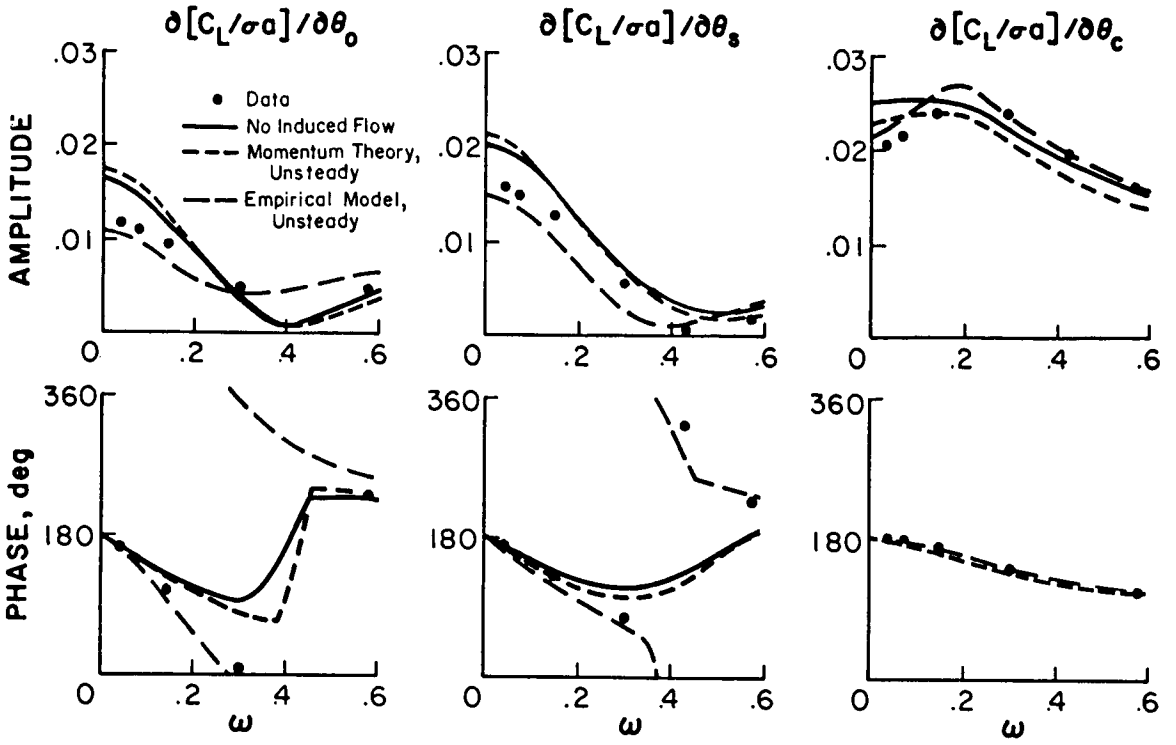

Figure 9. Rotor Response to Cyclic Pitch in Forward Flight, p=1.15, γ=4.25, B=.97, e_{pc}=.25, μ=.51, σa=.7294, $\bar{\nu}=\bar{\lambda}=0$, e_o=1/2", single rotating mode.

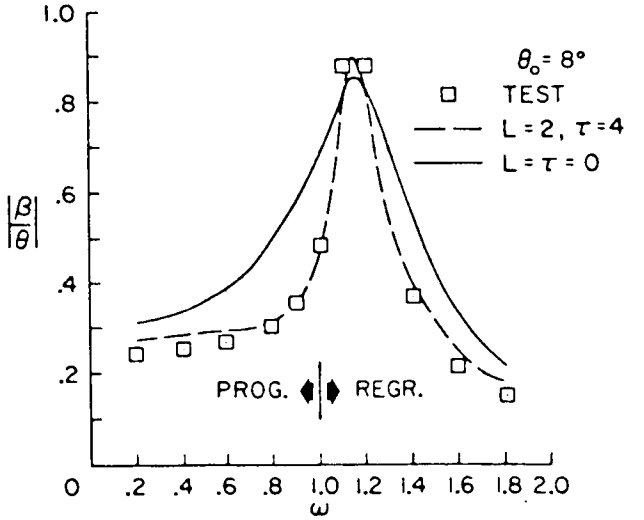

Figure 10. Rotor Response to Pitch Stirring, p=1.21, γ=4.0, ν=0, B=.97.

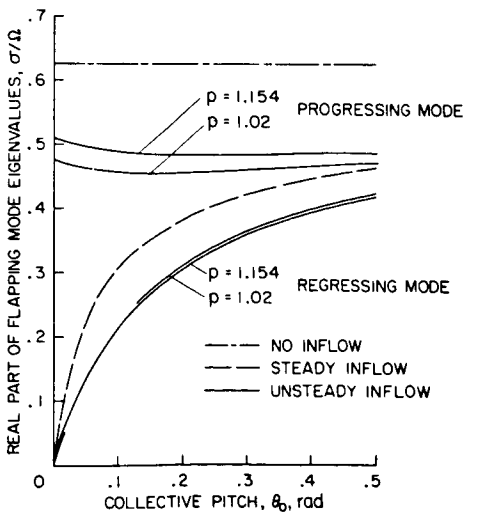

Figure 11. The Effect of Different Induced Flow Models on Flap Mode Damping, γ=10, σ=.15.

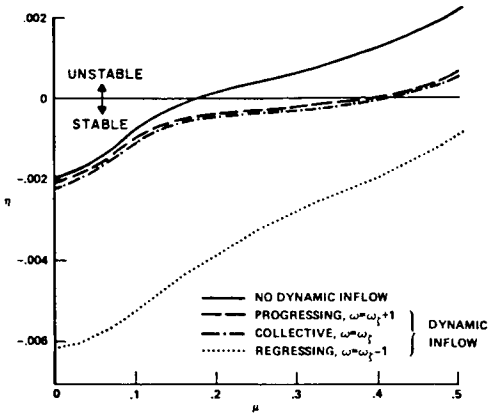

Figure 12. Effect of Dynamic Inflow on Lead-Lag Mode, ω_ζ =1.4, p=1.15, γ =5, C_T=0.1, σ =.05, C_{d_0}=.01.

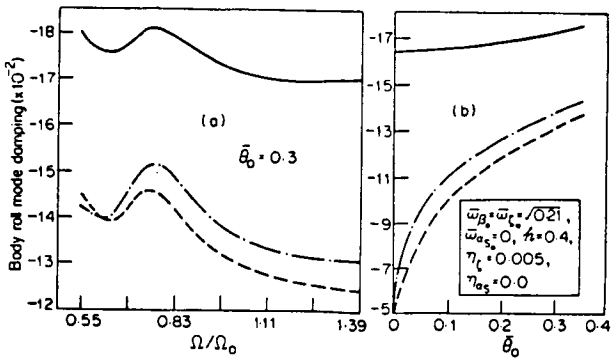

Figure 13.

Body Role Mode Damping of a Matched-Stiffness Rotor with: No Dynamic Inflow (—), Quasi-steady Inflow (—·—), and Unsteady Inflow (- - -); μ =.1, γ =5, σ =.05, p=1.1.

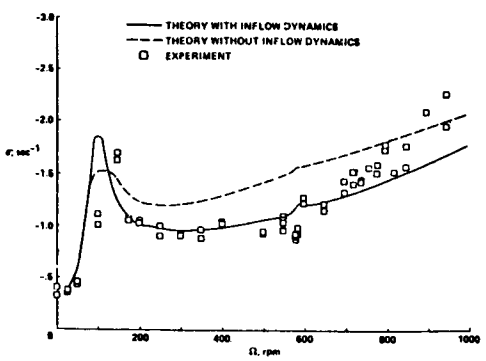

Figure 14.

Body Pitch Mode Damping as a Function of Rotor Speed, σ =.05, γ =8.4, Hover.

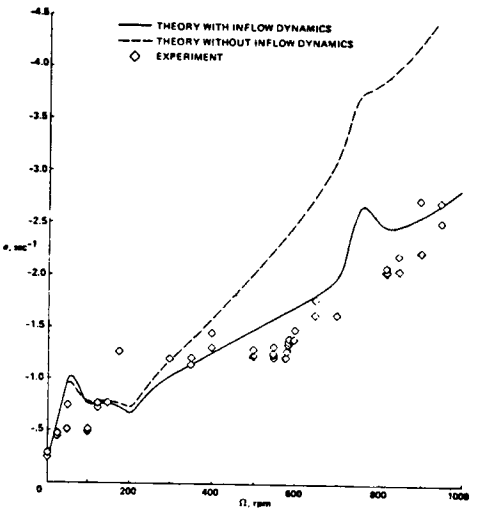

Figure 15.

Body Roll Mode Damping as a Function of Rotor Speed, σ =.05, γ =8.4, Hover.

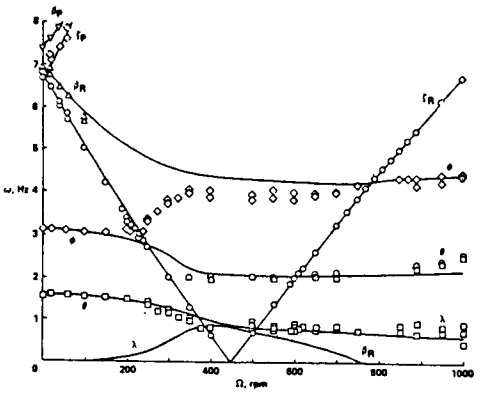

Figure 16.

Modal Frequencies as a Function of Rotor Speed: Comparison, Theory (—) and Data (o, ◇, □), σ =.05, γ = 8.4, Hover.

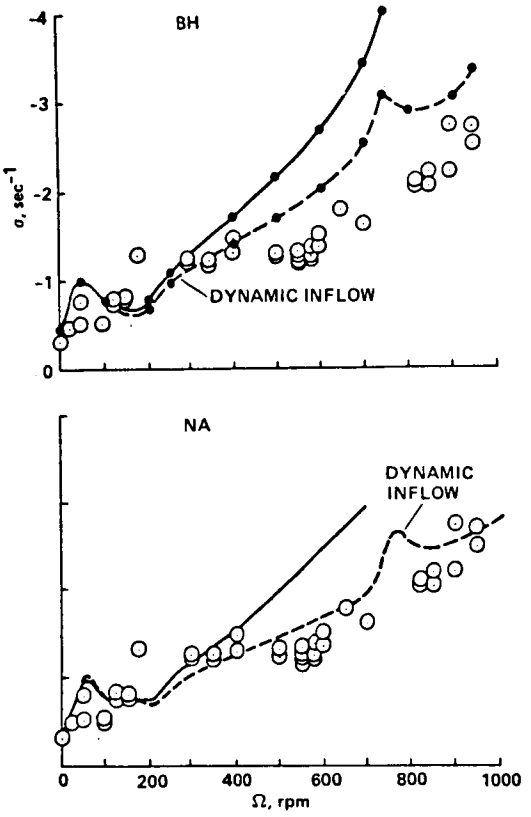

Figure 17. Comparison of Roll Mode Damping, Bell and NASA Ames Models.

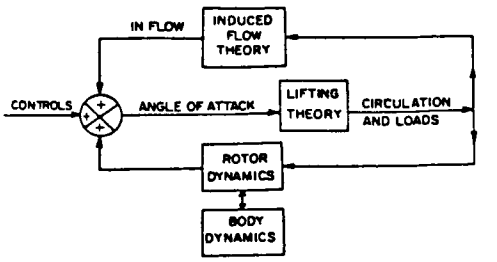

Figure 18. Block Diagram of Inflow Dynamics.

Figure 19.

Ellipsoidal Coordinates.

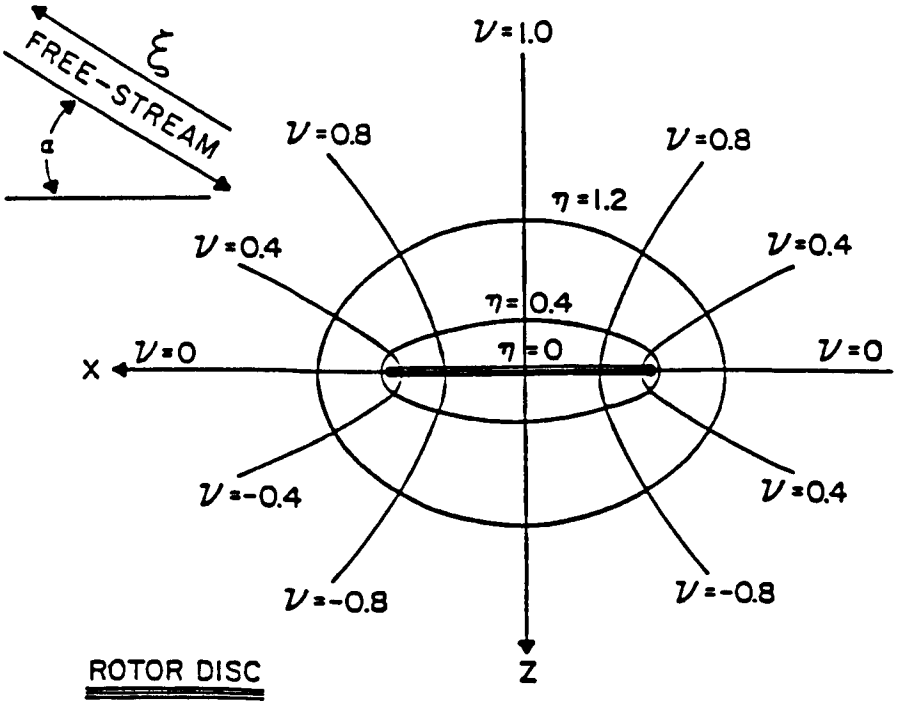

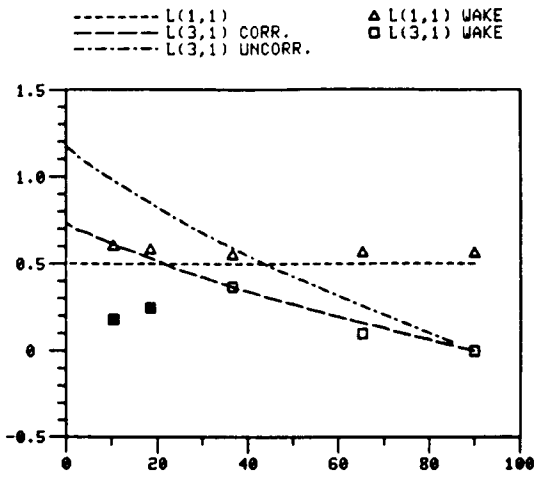

Figure 20. Verification of First Column of L.

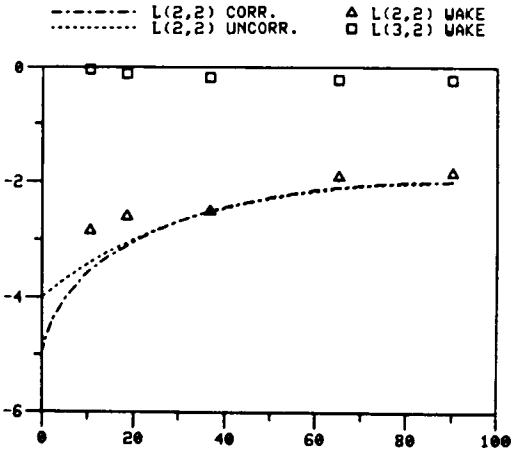

Figure 21. Verification of Second Column of L.

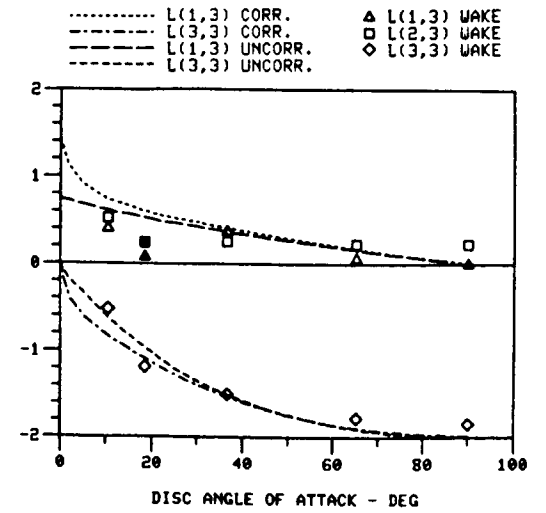

Figure 22. Verification of Third Column of L.

ORIGINAL PAGE IS
OF POOR QUALITY

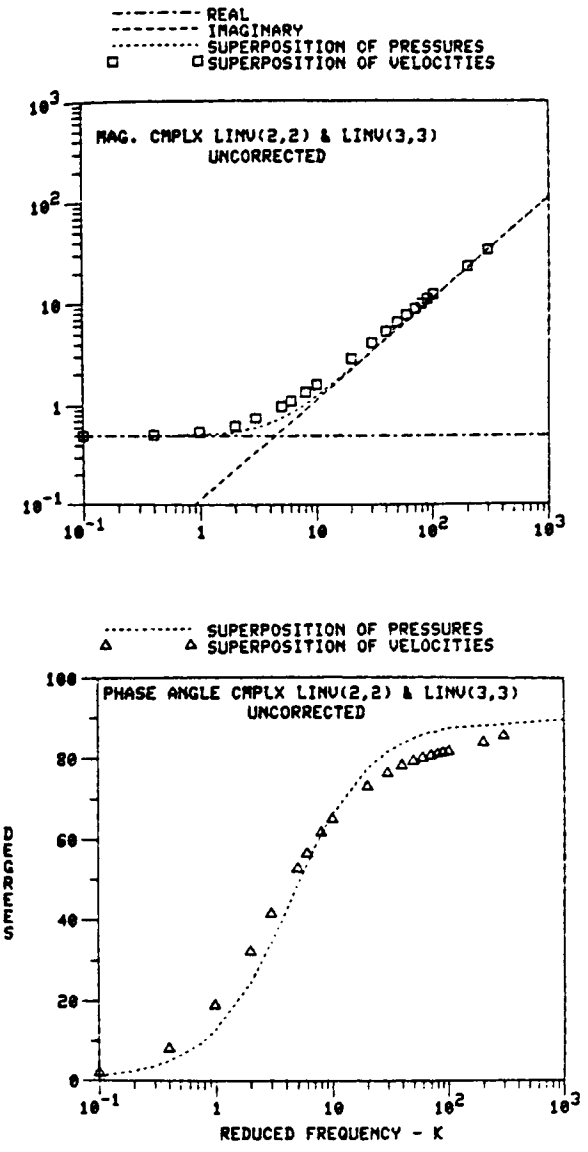

Figure 23.

Comparison of Unsteady Pressure Distribution with Superposition of Apparent Mass Terms.

Table 1. Comparison of Mass Flow Parameters

Condition	$\upsilon^* + \bar{\nu} \sin\alpha^*$ Ref. 11	$\upsilon + \bar{\nu} \sin\alpha$ Ref. 8	$\upsilon^* + \lambda + \bar{\nu}$ Ref. 20, C_T	υ^* Ref. 20, C_L and C_M
Hover, $\mu = \lambda = 0$	$2\bar{\nu}$	$2\bar{\nu}$	$2\bar{\nu}$	$\bar{\nu}$
Zero lift, climb $\bar{\nu} = 0$, $\mu = 0$	λ	λ	2λ	λ
Climb, $\mu = \upsilon$	$\lambda + 2\bar{\nu}$	$\lambda + 2\bar{\nu}$	$2\lambda + 2\bar{\nu}$	$\lambda + \bar{\nu}$
Zero lift, edgewise $\bar{\nu} = 0$, $\lambda = 0$	μ	μ	μ	μ
Lifting, edgewise $\lambda = 0$	$\frac{\mu^2 + 2\bar{\nu}^2}{\sqrt{\mu^2 + \bar{\nu}^2}}$	μ	$\sqrt{\mu^2 + \bar{\nu}^2} + \bar{\nu}$	$\sqrt{\mu^2 + \bar{\nu}^2}$
Zero lift $\bar{\nu} = 0$	$\sqrt{\mu^2 + \lambda^2}$	$\sqrt{\mu^2 + \lambda^2}$	$\sqrt{\mu^2 + \lambda^2} + \lambda$	$\sqrt{\mu^2 + \lambda^2}$
No normal flow, $\lambda = -\bar{\nu}$ (descent)	μ	$\frac{\mu^2 - \lambda^2}{\sqrt{\mu^2 + \lambda^2}}$	μ	μ

$$[L] = \frac{1}{v}\begin{bmatrix} \frac{1}{2} & 0 & \frac{15\pi}{64}\sqrt{\frac{1-\sin\alpha}{1+\sin\alpha}} \\ 0 & \frac{-4}{1+\sin\alpha} & 0 \\ \frac{15\pi}{64}\sqrt{\frac{1-\sin\alpha}{1+\sin\alpha}} & 0 & \frac{-4\sin\alpha}{1+\sin\alpha} \end{bmatrix}$$

$$[M] = \begin{bmatrix} \frac{128}{75\pi} & 0 & 0 \\ 0 & \frac{-16}{45\pi} & 0 \\ 0 & 0 & \frac{-16}{45\pi} \end{bmatrix}$$

Table 2. Analytic Forms of L-matrix and M-matrix

$$[L] = [\mathcal{L}]\begin{bmatrix} 1/V_T & 0 & 0 \\ 0 & 1/V & 0 \\ 0 & 0 & 1/V \end{bmatrix}$$

$$V_T = \sqrt{(\lambda+v_0)^2+\mu^2} \qquad V = \frac{d}{dv_0}(v_0 V_T)$$

$$V = \left[(\lambda+v_0)(\lambda+2v_0)+\mu^2\right]/V_T$$

Table 3. Nonlinear Version of Dynamic Inflow Theory